buildings

MDPI

Article

Study on Performance Optimization of Red Mud–Mineral Powder Composite Cementitious Material Based on Response Surface Methodology

Chao Yang [1,*], Qiang Zeng [2], Jun Hu [2] and Wenbo Zhu [3]

[1] Yangzhou Polytechnic Institute, Yangzhou 225127, China
[2] School of Civil Engineering and Architecture, East China Jiaotong University, Nanchang 330013, China; 2024018085901127@ecjtu.edu.cn (Q.Z.); 2024018085901082@ecjtu.edu.cn (J.H.)
[3] School of Civil Engineering, Southeast University, Nanjing 210096, China; 101300143@seu.edu.cn
* Correspondence: yangc@ypi.edu.cn

Abstract

Red mud, a highly alkaline industrial by-product generated during aluminum smelting, poses serious environmental risks such as soil alkalization and ecological degradation. In this study, response surface methodology (RSM) was integrated with advanced microstructural characterization techniques to optimize the performance of red mud–slag composite cementitious materials through multi-factor analysis. By constructing a four-factor interaction model—including red mud content, steel fiber content, alkali activator dosage, and calcination temperature—a systematic mix design and performance prediction framework was established, overcoming the limitations of traditional single-factor experimental approaches. The optimal ratio was determined via multi-factor RSM analysis as follows: the 28-day flexural strength and compressive strength of the specimens reached 12.26 MPa and 69.83 MPa, respectively. Furthermore, XRD and SEM-EDS analyses revealed the synergistic formation of C-S-H and C-A-S-H gels, and their strengthening effects at the fiber–matrix interfacial transition zone (ITZ), elucidating the micro-mechanism pathway of "gel densification–rack filling–strength enhancement." This work not only enriches the theoretical foundation for the design of red mud-based binders but also offers practical insights and empirical evidence for their engineering applications, highlighting substantial potential in the development of sustainable building materials and high-value utilization of industrial solid waste.

Keywords: red mud; mineral powder; alkali excitation; response surface methodology (RSM); cementitious material

check for updates

Academic Editor: Antonio Caggiano

Received: 27 May 2025
Revised: 19 June 2025
Accepted: 26 June 2025
Published: 3 July 2025

Citation: Yang, C.; Zeng, Q.; Hu, J.; Zhu, W. Study on Performance Optimization of Red Mud–Mineral Powder Composite Cementitious Material Based on Response Surface Methodology. *Buildings* **2025**, *15*, 2339. https://doi.org/10.3390/buildings15132339

Copyright: © 2025 by the authors. Licensee MDPI, Basel, Switzerland. This article is an open access article distributed under the terms and conditions of the Creative Commons Attribution (CC BY) license (https://creativecommons.org/licenses/by/4.0/).

1. Introduction

Red mud, a highly alkaline industrial by-product generated during aluminum smelting, is generated at approximately 0.8 to 1.5 tons per ton of alumina produced. Currently, China's annual red mud output is close to 120 million tons, but its resource utilization rate is less than 8%, far below the average level of other industrial solid wastes [1–4]. Red mud is typically disposed of by wet stacking, characterized by strong alkalinity and high heavy-metal content. Under the leaching action of rainwater, it easily causes soil alkalization and groundwater pollution, leading to ecosystem degradation and reduction in agricultural production [5]. Therefore, improving the resource utilization efficiency of red mud has become an urgent need.

To address the above challenges, multiple departments including the Ministry of Industry and Information Technology issued the Action Plan for Comprehensive Utilization of Red Mud in 2024, proposing that the comprehensive utilization rate of red mud should reach 15% and 25% by 2027 and 2030, respectively. The introduction of this policy provides new opportunities for the efficient utilization of red mud [6]. In the research on the resource utilization of red mud, Tsakiridis P E et al. [7] studied the influence of Bayer red mud on the performance of Portland cement clinker. The results showed that the sample with 3.5% red mud addition achieved a compressive strength of 45 MPa after 28 days of hydration, meeting industrial standard requirements. Zhu et al. [8] significantly improved the dealkalization rate of red mud through CaO dealkalization treatment, providing a basis for the further application of red mud in cement clinker preparation. He Mingda et al. [9] successfully prepared Portland cement by mixing red mud and copper slag at a 1:1 ratio, achieving an excellent 28-day compressive strength of 63.2 MPa. The research by Garanayakl et al. [10] showed that when slag and red mud are mixed at a mass ratio of 1:1, the hydration strength of the prepared slag cement is comparable to that of ordinary Portland cement. Zhao Yanrong et al. [11] successfully prepared belite sulphoaluminate cement using fly ash and Bayer red mud as the main raw materials. The experimental results showed that when the red mud content is 4%, the 28-day compressive strength of the cement can reach 48.9 MPa. Ren C et al. [12] found that using industrial solid wastes such as red mud and desulfurized gypsum to prepare sulphoaluminate cement clinker not only reduces CO_2 emissions by 42.1%, energy consumption by 8.3%, but also decreases the comprehensive environmental impact by 38.62%. Liu Juanhong et al. [13] combined Bayer red mud with fly ash, and added a small amount of desulfurized gypsum, lime, and an activator to prepare mine backfill materials. The study found that the addition of desulfurized gypsum and lime promoted the formation of ettringite, and the activator accelerated the hydration of the red mud-fly ash cementitious material. The main hydration products were ettringite and silicoaluminate gel.

Therefore, in terms of the technical method, existing studies [14–16] mostly rely on single-factor optimization or empirical proportioning design, failing to reveal the interaction effects among multiple factors such as red mud content and fiber content. In mechanism research, most studies stay at the macro-performance testing level, lacking an analysis of the micro-coupling mechanism of C-S-H gel and steel fiber bridging effect. Steel fiber–reinforced concrete has been widely employed in high-performance concrete and specialty materials because of its superior crack resistance, toughness, and durability. Prior studies have shown that steel fibers markedly enhance the composite's flexural and impact resistance by bridging cracks, inhibiting their propagation, and strengthening the interfacial transition zone [17,18]. Thus, to enhance the application potential of red mud-based cementitious materials, it is urgent to introduce multi-factor analysis tools such as RSM to clarify the influence of trends in various factors and their interactions on performance and combine microscopic analysis methods to reveal the gelation mechanism.

Thus, this paper takes red mud and mineral powder as the main raw materials to prepare red mud–mineral powder composite cementitious materials. The combination of RSM and microscopic characterization technology is adopted to construct an interaction model of four factors (red mud content, fiber content, alkali activator content, and calcination temperature), breaking through the parameter exploration limitations of traditional single-factor tests. Meanwhile, the material is expected to achieve a compressive strength of $\geq$12 MPa and a flexural strength of $\geq$65 MPa at 28 d. The composition of hydration products is analyzed by XRD, and the microstructural evolution process is observed by SEM to discuss the gelation mechanism and strength development law under different proportion conditions. The research in this paper not only provides new ideas and technical

paths for the efficient resource utilization of red mud, a typical industrial solid waste, but also has important engineering practical significance and environmental protection value.

2. Experimental Materials and Methods

2.1. Experimental Materials

The primary materials used in this experiment include red mud, ground granulated blast-furnace slag (GGBS), water glass solution, and granular NaOH. The sources of these materials are listed in Table 1. The red mud has a density of 1650 kg/m^3. Due to the variation in particle size, the red mud samples were ground using a ball mill for 5 min to ensure uniformity. Subsequently, the samples were subjected to calcination at heating rates of 5 °C/min, and held at target temperatures of 650 °C, 750 °C, and 850 °C for durations of 1.5 h and 2.5 h, respectively. The GGBS used was S95-grade slag powder produced by Xintang County Xinlei Mineral Powder Processing Plant (Table 2) with a density of 2700 kg/m^3. The hooked-end steel fibers used were standard short straight (SS) fibers with a length-to-diameter ratio (l/d) of 65, manufactured by Bekaert (Shanghai). The geometric and physical properties of the fibers are listed in Table 3. To enhance the mechanical performance of the composite, end-hooked copper-plated steel fibers were incorporated. Granular NaOH and liquid sodium silicate (water glass) were employed as alkali activators. The water glass contained 26.98% SiO_2 and 8.53% Na_2O with an initial modulus of 3.2 (Table 4). The molar ratio of SiO_2 to Na_2O in water glass is a critical parameter that reflects the alkalinity and the silica supply capacity of the activator. The NaOH used was analytical grade with a purity of ≥96% and was applied to adjust the modulus of the activator to meet the requirements of different test conditions. Details of the testing instruments and equipment are provided in Table 5.

Table 1. Sources of test materials.

Serial Number	Material	Enterprise	Location
1	Red mud	Shandong Weiqiao Aluminum Co., Ltd.	Binzhou, China
2	Slag powder	Tang County Xinlei Mineral Powder Processing Plant	Baoding, China
3	Water glass	Nantong Yourui Building Materials Trading Co., Ltd.	Nantong, China
4	NaOH	Xilong Scientific Co., Ltd.	Shantou, China

Table 2. Main chemical composition of red mud and slag.

Type	SiO_2	Al_2O_3	Fe_2O_3	Na_2O	SO_3	TiO_2	CaO	MgO	K_2O	Others
Red mud	15.30	25.32	41.02	11.03	0.68	5.21	0.56	0.17	0.18	0.53
Slag powder	31.75	18.94	-	0.62	-	0.98	33.15	10.32	0.38	3.86

Table 3. Geometric and physical properties of steel fiber.

Type of Fiber	Length/mm	Diameter/mm	Length Diameter Ratio L/d	Density/(g.cm^{-3})	Elastic Modulus/GPa	Tensile Strength/MPa
SS	14	0.2	63	7.8	201	≥2700

Table 4. Parameters and indicators of sodium silicate solution.

Modulus	Na_2O	SiO_2	pH	Density(g/cm^3)	Baumé Degree/(°Be)
3.26	8.53	26.98	10~13	5.42	38.5

Table 5. Details of test instruments and equipment.

Serial Number	Name	Model	Manufacturer	Location
1	Electronic Balance	HZ-20003	Kunshan Hua'e Electronic Technology Co., Ltd.	Kunshan, China
2	Planetary Ball Mill	YXQM	Changsha Mimi Instrument Equipment Co., Ltd.	Changsha, China
3	Muffle Furnace	SX2-18-12A	Shaoxing Daoxu Yanguang Instrument Equipment Factory	Shaoxing, China
4	Constant Temperature and Humidity Curing Chamber	GH	Guangheng Sibo Testing Equipment Co., Ltd.	Shanghai, China
5	Constant Loading Pressure Testing Machine	TYA-2000A	Wuxi Jianyi Laboratory Equipment Co., Ltd.	Wuxi, China
6	Electric Hot Air Drying Oven	SN-101-4B	Shangyi Scientific Instruments Co., Ltd.	Shaoxing, China
7	Vibration Table	HZJ-A	Hebei Junyi Instrument Factory	Cangzhou, China
8	Mixer	JJ-5	Shangyu Yueda Instrument Factory	Shaoxing, China
9	X-ray Diffractometer	D/MAX-IIIA	Dandong Haoyuan Instrument Co., Ltd.	Dandong, China
10	Scanning Electron Microscope	HITACHI-SU8010	Nisshin Science Instruments Co., Ltd.	Guangzhou, Japan

2.2. Experimental Scheme

In this study, Design-Expert 13 software was used to implement RSM. The RSM module of this software was utilized to design, analyze, and optimize the mix proportion of the red mud–mineral powder composite cementitious material. In the response surface methodology, the number of experimental points is intrinsically related to the number of independent variables, and the spatial arrangement of these design points critically influences model fidelity. The Box–Behnken design strategy strategically optimizes the configuration of sampling points to minimize experimental iterations while preserving predictive accuracy. Specifically, the quantitative relationship between the number of factors (k) and the total required experimental runs (n) can be mathematically expressed through Equation (1).

$$n = m_c + m_a + m_0 \quad (1)$$

where n is the number of experimental points; m_c is the number of permutations when each factor takes the values of 1 and -1, $m_c = 2^k$; m_a is the number of test points on the coordinate axes, $m_a = 2k$; m_0 is the number of repeated tests at the central point where all factors are at the 0 level, with a default value of 5 for Box–Behnken response surface methodology tests.

The experiment first designed a four-factor, three-level scheme based on the RSM, selecting red mud content (A), hooked copper-plated steel fiber content (B), alkali activator

dosage (C), and red mud calcination temperature (D) as the four factors, with three levels for each factor: red mud content at 5%, 10%, and 15%; hooked copper-plated steel fiber at 0, 0.75 vol.%, and 1.5 vol.%; alkali activator dosage at 12%, 16%, and 20%; red mud calcination temperature at 650 °C, 750 °C, and 850 °C. Then, alkali-activated red mud cementitious material specimens with dimensions of 40 × 40 × 160 mm were prepared. The total amount of binder in the specimens consisted of red mud and mineral powder, with their admixture ratios summing to 100%. The modulus of the alkali activator was set to 1.5, and its dosage was calculated as a mass fraction of the binder. Meanwhile, the binder-to-aggregate ratio of the specimens was 1:3, and the water-to-binder ratio was 0.3.

Subsequently, the mechanical properties of each group of specimens were measured using standardized testing equipment, and the experimental data were input into analysis software for regression modeling. Through the analysis of response surface contour plots and interaction diagrams, the influence of mix proportion parameters on material properties were intuitively displayed. Finally, an optimization algorithm was used to determine the optimal mix proportion. Table 6 shows the specific experimental design scheme and corresponding test results.

Table 6. Four-factor third-order response surface test ratio and results.

Group Number	Factors				Test Results	
	The Dosage of Red Mud/% (A)	End-Hook Copper-Plated Steel Fiber /vol.% (B)	Dosage of Alkali Activator /% (C)	The Calcination Temperature of Red Mud /°C (D)	28-Day Compressive Strength /MPa (Y1)	28-Day Flexural Strength /MPa (Y2)
1	15	1.5	16	750	75.19	7.86
2	15	0.75	16	650	77.07	7.88
3	10	0	16	850	69.83	12.26
4	10	0.75	16	750	74.16	11.85
5	10	0	20	750	69.08	6.25
6	10	1.5	16	650	70.89	11.14
7	5	0.75	20	750	57.94	6.72
8	15	0.75	16	850	65.56	8.38
9	10	0.75	20	650	76.29	7.3
10	10	1.5	16	850	77.14	13.26
11	10	0	12	750	56.08	8.88
12	5	0.75	12	750	54.18	8.7
13	10	0.75	16	750	73.56	11.13
14	10	0.75	12	850	56.55	9.36
15	5	0	16	750	67.44	9.63
16	10	0	16	650	72.43	9.76
17	10	0.75	16	750	76.91	12.12
18	5	1.5	16	750	66.79	15.03
19	10	1.5	20	750	75.43	8.9
20	5	0.75	16	650	58.93	9.26
21	15	0	16	750	69.93	10.51
22	15	0.75	20	750	82.93	5.38
23	15	0.75	12	750	54.42	6.9
24	10	0.75	16	750	72.65	11.34
25	5	0.75	16	850	65.38	11.18
26	10	0.75	16	750	70.61	12.04
27	10	1.5	12	750	54.53	9.56
28	10	0.75	20	850	69.06	6.96
29	10	0.75	12	650	57.94	7.84

2.3. Experimental Methods

2.3.1. Mechanical Property Test

The tests were carried out in accordance with the standard Test Method for Strength of Cement Mortar (ISO) [19] (GB/T 17671-2021). This standard was equivalently adopted from the international standard ISO 679:2009 methods of testing cement—Determination of strength [20]. The specimens were rectangular prisms with dimensions of 40 mm × 40 mm × 160 mm, and 3 specimens were tested in each group. The test was conducted using a TYA-2000A-type

constant-loading pressure testing machine. For the compression test, displacement control was adopted, and the loading rate was 1.3 mm/min. For the flexural test, also using displacement control, the loading rate was 0.12 mm/min.

2.3.2. XRD Test

The XRD test was performed using a D/MAX-IIIA diffractometer with a Cu Kα radiation source (λ = 1.5406 Å). The operating voltage and current were set at 40 kV and 40 mA, respectively. The test parameters were as follows: scanning rate of 2°/min, step size of 0.02°, and scanning range of 2θ from 5° to 90°. The 3rd sample of the test group was selected to determine the phase composition on the 3rd, 7th, and 28th day.

2.3.3. SEM Test

The microstructure of red mud–mineral powder composite cementitious materials was observed using a HITACHI SU8010 SEM, and the formation mechanism of its mechanical properties was analyzed. Before testing, the samples were polished and sputter-coated with gold, and the testing voltage was set at 20 kV. The 3rd sample of the test group was selected for observation to analyze the microstructures of samples on the 3rd, 7th, and 28th day.

3. Results and Discussion

3.1. Analysis of Variance for the Regression Model

According to the principles of response surface design and the experimental results, second-order polynomial regression models were established in coded form, as presented in Equations (2) and (3).

$$\begin{aligned} y_1 = \; & 73.58 + 4.54A + 1.26B + 8.09C - 0.8358D + 1.48AB + 6.19AC \\ & -4.49AD + 1.98BC + 2.21BD - 1.46CD - 4.03A^2 - 0.4027B^2 \\ & -7.94C^2 - 1.36D^2 \end{aligned} \quad (2)$$

$$\begin{aligned} y_2 = \; & 11.5 - 1.27A + 0.8717B - 0.8108C + 0.385D - 2.01AB + 0.115AC \\ & -0.755AD + 0.4925BC + 0.905BD - 0.465CD - 1.41A^2 + 0.2445B^2 \\ & -3.04C^2 - 1.01D^2 \end{aligned} \quad (3)$$

The analysis of variance for the regression model was conducted to evaluate the contribution of each independent variable to the overall variability, thereby determining the significance of factors influencing the mechanical properties of alkali-activated red mud–mineral powder composite cementitious materials [21]. In the regression models obtained via response surface methodology, a larger F-value and a smaller *p*-value indicate a more significant influence of the variable on the response [22,23]. Specifically, a *p*-value $\leq$ 0.05 denotes statistical significance at the 95% confidence level, while $p \leq 0.001$ indicates a highly significant correlation and strong model reliability. Conversely, a *p*-value > 0.05 suggests limited predictive capability. The correlation coefficient (R) and the coefficient of determination (R^2) are used to assess the model's goodness-of-fit, with an R^2 value approaching one indicating strong agreement between predicted and observed values and high explanatory power. The *p*-value for lack-of-fit is used to evaluate whether the model adequately fits the data; a value greater than 0.5 suggests that the lack-of-fit is not significant and the model is appropriate for describing the response surface.

Table 7 presents the results of the analysis of variance (ANOVA), evaluating the significance of experimental factors on the 28-day flexural strength (y_1) and compressive strength (y_2). The F-values of the models are 28.09 and 19.42, respectively, with corresponding *p*-values of less than 0.0001, indicating that both models are highly significant and can

reliably describe the relationship between the response variables and the input factors. Among the main effects, factors A (red mud content) and C (alkali activator dosage) exhibit extremely significant influence on both y_1 and y_2 ($p < 0.0001$). Factor B (steel fiber content) significantly affects y_1 ($p = 0.0012$) but shows no significant effect on y_2 ($p = 0.1119$). Factor D (calcination temperature of red mud) shows lower significance for both response variables. The interaction term AB significantly affects y_1 ($p < 0.0001$) but not y_2 ($p = 0.2718$). The quadratic terms A^2 and C^2 display highly significant nonlinear effects on both y_1 and y_2 ($p < 0.0001$). Some interaction terms, such as BC and CD, exhibit varying degrees of significance, suggesting complex interdependencies among the experimental factors.

Table 7. Analysis of variance for the quadratic polynomial regression model.

Variation Source	Sum of Squares		Degrees of Freedom		Mean Square		F-Value		*p*-Value	
	y_1	y_2	y_1	y_2	y_1	y_2	y_1	y_2	y_1	y_2
Model	142.74	1813.94	14	14	10.20	129.57	28.09	19.42	<0.0001	<0.0001
A	15.44	246.98	1	1	15.44	246.98	42.53	37.02	<0.0001	<0.0001
B	5.96	19.2	1	1	5.96	19.2	16.43	2.88	0.0012	0.1119
C	7.89	784.57	1	1	7.89	784.57	21.74	117.61	0.0004	<0.0001
D	5.63	8.38	1	1	5.63	8.38	15.51	1.26	0.0015	0.2811
AB	16.20	8.73	1	1	16.20	8.73	44.64	1.31	<0.0001	0.2718
AC	0.0529	153.14	1	1	0.0529	153.14	0.1458	22.96	0.7084	0.0003
AD	0.5041	80.64	1	1	0.5041	80.64	1.39	12.09	0.2582	0.0037
BC	0.9702	15.6	1	1	0.9702	15.6	2.67	2.34	0.1243	0.1485
BD	0.0361	19.58	1	1	0.0361	19.58	0.0995	2.94	0.7571	0.1087
CD	0.8649	8.53	1	1	0.8649	8.53	2.38	1.28	0.1450	0.2772
A^2	15.39	105.23	1	1	15.39	105.23	42.39	15.77	<0.0001	0.0014
B^2	1.10	1.05	1	1	1.10	1.05	3.02	0.1577	0.1041	0.6973
C^2	73.89	409.34	1	1	73.89	409.34	203.59	61.36	<0.0001	<0.0001
D^2	2.71	12.07	1	1	2.71	12.07	7.47	1.81	0.0162	0.2

Table 8 further evaluates the goodness-of-fit of the second-order polynomial regression models. The coefficients of determination (R^2) for flexural strength (y_1) and compressive strength (y_2) are 0.9656 and 0.9510, respectively, indicating excellent model fitting and strong agreement between the predicted and observed values. The differences between the adjusted R^2 (R^2_{adj}) and predicted R^2 (R^2_{pred}) values are both less than 0.2, suggesting good consistency between model calibration and prediction performance.

Table 8. Analysis of fit precision.

Response Value	R^2	R^2_{adj}	R^2_{pred}	C.V./%	Signal-to-Noise Ratio
7d Flexural Strength (y_1)	0.9656	0.9313	0.8238	6.30	21.8521
7d Compressive Strength (y_2)	0.9510	0.9021	0.7644	3.80	15.3677

Moreover, the coefficients of variation (C.V.%) for the models are 6.30% and 3.80%, respectively—both below the 10% threshold—implying high experimental reliability. The signal-to-noise ratios are 21.8521 for y_1 and 15.3677 for y_2, both substantially greater than four, indicating that the models exhibit strong robustness against experimental noise and are capable of reliably capturing the relationships between the input factors and response variables under complex conditions.

In summary, the second-order polynomial regression models effectively characterize the effects of experimental factors on the 28-day flexural and compressive strengths of

alkali-activated red mud–mineral powder composite cementitious materials. Both the significance analysis and goodness-of-fit metrics confirm that the models are statistically robust and practically applicable.

3.2. Analysis of Response Surface Model Prediction Accuracy

Figure 1 presents the residual analysis results of the 28-day flexural strength and compressive strength for the red mud–mineral powder composite cementitious material. Residual analysis serves as a critical method for evaluating the fitting effectiveness of regression models, enabling validation of model relevance and experimental data reliability. Under ideal conditions, residuals should follow a normal distribution without significant systematic deviations. As shown in the figure, the standardized residuals of flexural strength fall within the range of ±2, while those of compressive strength are confined within ±2. This indicates a strong correlation between experimental data points and model fitting, demonstrating reasonable selection of test points and credible experimental results. Furthermore, residual points on the normal probability plot exhibit near-linear distribution with minimal outliers, confirming that residuals conform to a normal distribution. These findings collectively validate the high fitting accuracy of the regression model, which effectively explain the variation patterns of compressive strength and flexural strength.

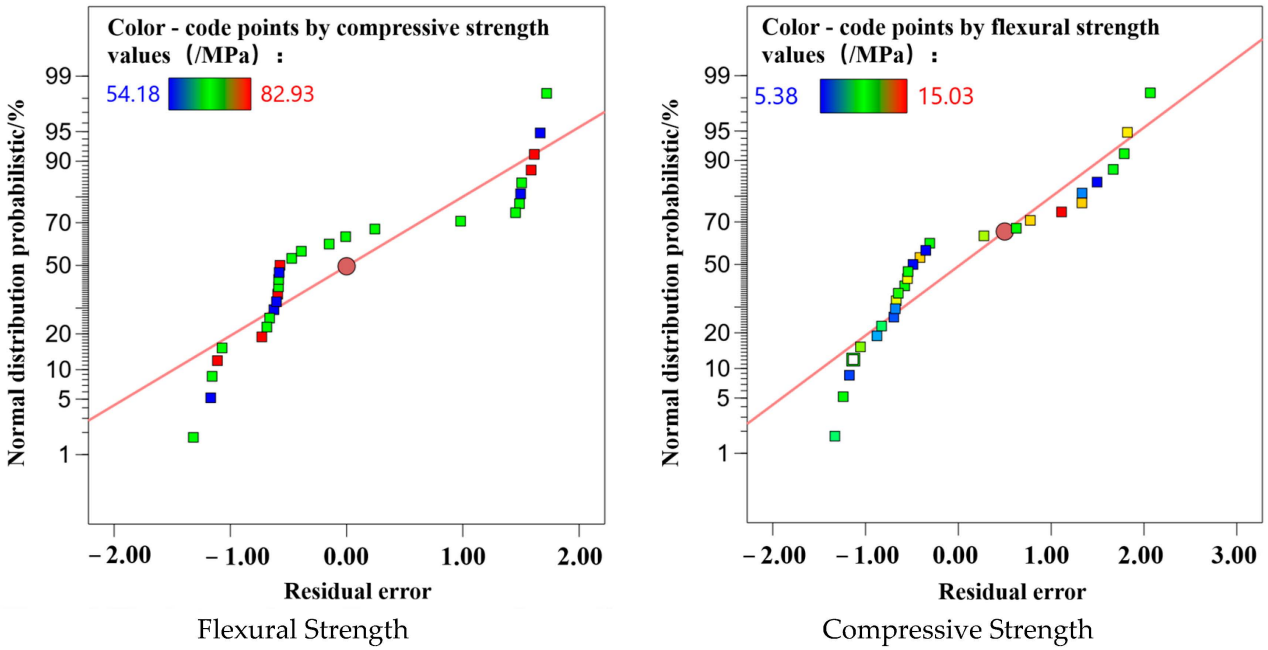


Figure 1. Residual analysis of 28-day flexural/compressive strength of specimens.

Figure 2 presents a comparative analysis between experimental and predicted values of the 28-day flexural strength and compressive strength for red mud cementitious material specimens. As shown in Figure 2, the distribution of experimental and predicted values closely follows the line y = x, with most data points either aligning tightly with the line or distributing symmetrically on both sides, indicating minimal deviations between predictions and actual measurements. The homogeneous scattering pattern without clustered outliers further verifies the high prediction accuracy of the model. Overall, the response surface regression model effectively captures the variation trends of compressive and flexural strengths of the specimens, demonstrating excellent fitting performance.

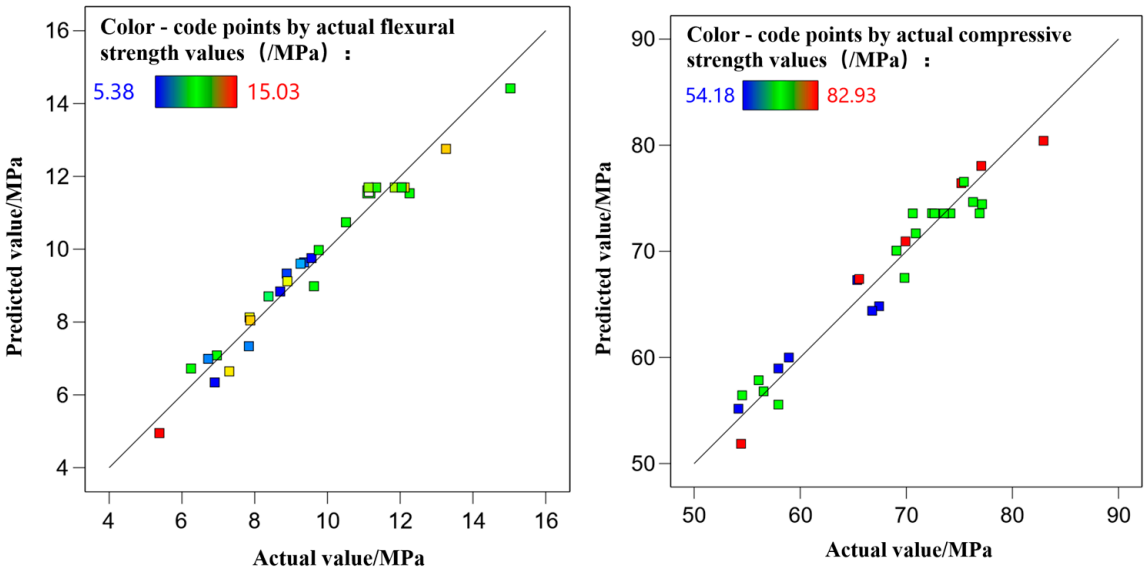


Figure 2. Analysis of predicted and actual values of 28-day flexural/compressive strength of samples.

Combined with residual analysis and predictive value comparisons, the developed model reliably interprets the effects of key factors—including red mud content, alkali activator dosage, and red mud calcination temperature—on the 28-day flexural and compressive strengths of the red mud–mineral powder composite cementitious material. The high consistency between experimental and predicted results confirms the model's robust fitting accuracy.

3.3. Analysis of Factors Influencing Mechanical Properties

3.3.1. Flexural Strength Analysis

Figure 3 demonstrates that at a fiber content of 0 vol%, the flexural strength of the material exhibits an initial increase followed by a decrease with varying alkali activator dosage and red mud content, regardless of the red mud calcination temperature (650 °C or 850 °C). The peak flexural strength is achieved at an alkali activator dosage of 16% and red mud content of approximately 11%.

When the fiber content increases to 1.5 vol%, the optimal mix proportion shifts significantly. At calcination temperatures of 650 °C and 850 °C, the maximum flexural strength is attained with an alkali activator dosage of 16.7% and red mud content of 5%. This phenomenon primarily stems from the effective toughening mechanism of fibers in crack bridging and stress distribution, which becomes fully operational under low red mud content conditions, thereby substantially enhancing flexural strength. Although variable B was originally set at three levels (0, 0.75, and 1.5 vol.%), the 0.75 vol.% data exhibited an intermediate, transitional response that did not introduce additional mechanistic trends beyond those captured by the two boundary levels. However, excessive fiber incorporation (>1.5 vol%) disrupts the homogeneity of the cementitious matrix, inducing localized stress concentration and consequently inhibiting further performance improvement [24].

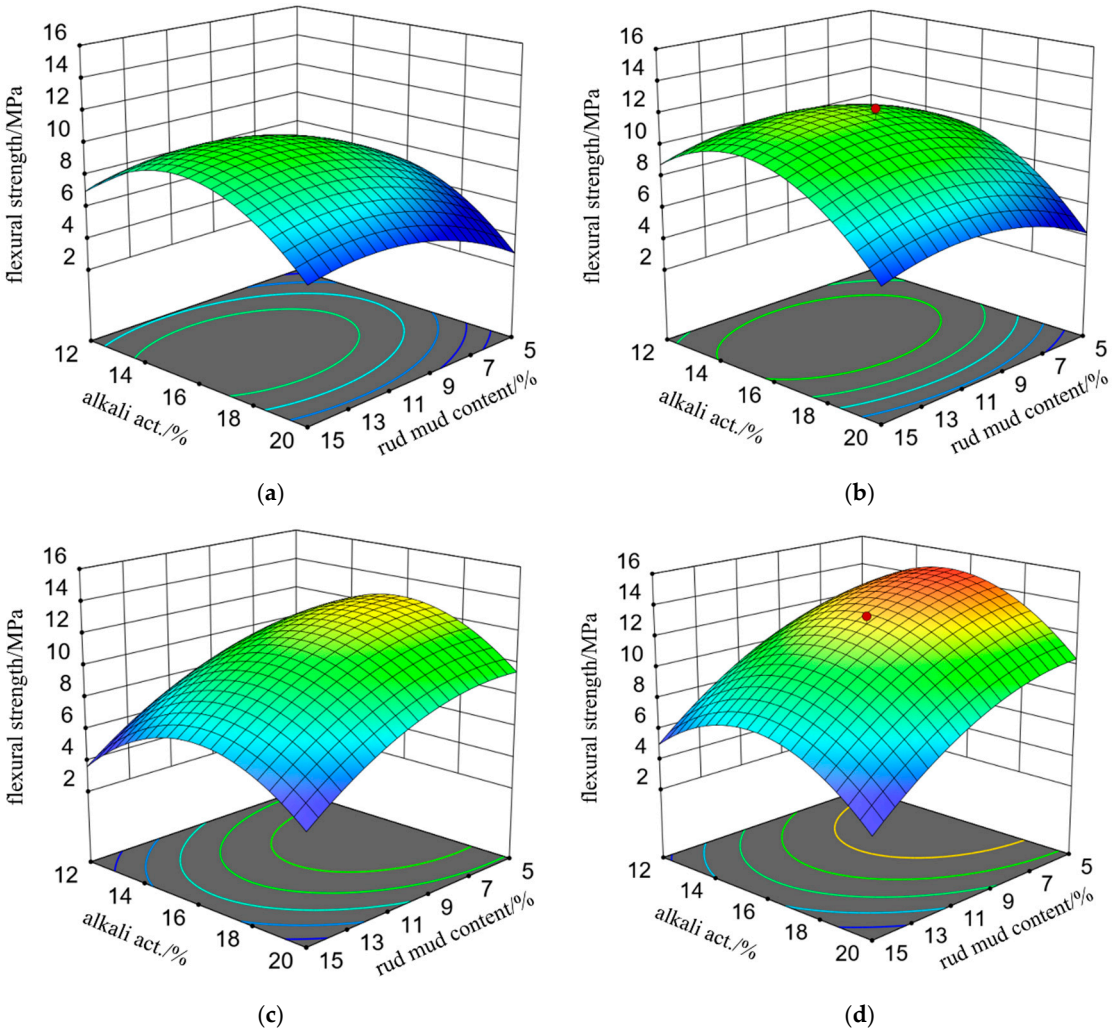


Figure 3. Effects of alkali activator and red mud content on 28-day flexural strength of samples under different conditions. Variable B denotes the volume content of end-hook copper-plated steel fibers (vol.%), and variable D represents the calcination temperature of red mud (°C). (**a**) B = 0; D = 650. (**b**) B = 0; D = 850. (**c**) B = 1.5; D = 650. (**d**) B = 1.5; D = 850.

3.3.2. Compressive Strength Analysis

Figure 4 reveals that at a fiber content of 0 vol% and a red mud calcination temperature of 650 °C, the optimal mix proportion for compressive strength is achieved with an alkali activator dosage of 20% and red mud content of 15%. This phenomenon primarily results from the sufficient activation of reactive components in red mud by the higher alkali activator dosage under lower calcination temperatures, promoting the formation of abundant cementitious products and significantly enhancing material densification and compressive strength. When the calcination temperature increases to 850 °C, the optimal parameters shift to an alkali activator dosage of 16% and red mud content of 9%. This indicates that elevated calcination temperatures further activate the reactivity of red mud, enabling notable strength improvement even at reduced material dosages, though excessive red mud content may inhibit performance enhancement. At a fiber content of 1.5 vol%, compressive strength increases with rising alkali activator dosage and red mud content under both 650 °C and 850 °C calcination conditions. The peak compressive strength is attained at an alkali activator dosage of 20% and red mud content of 15%. The incorporation of steel fibers contributes to crack bridging and toughness enhancement within the high-strength matrix, thereby markedly improving compressive performance.

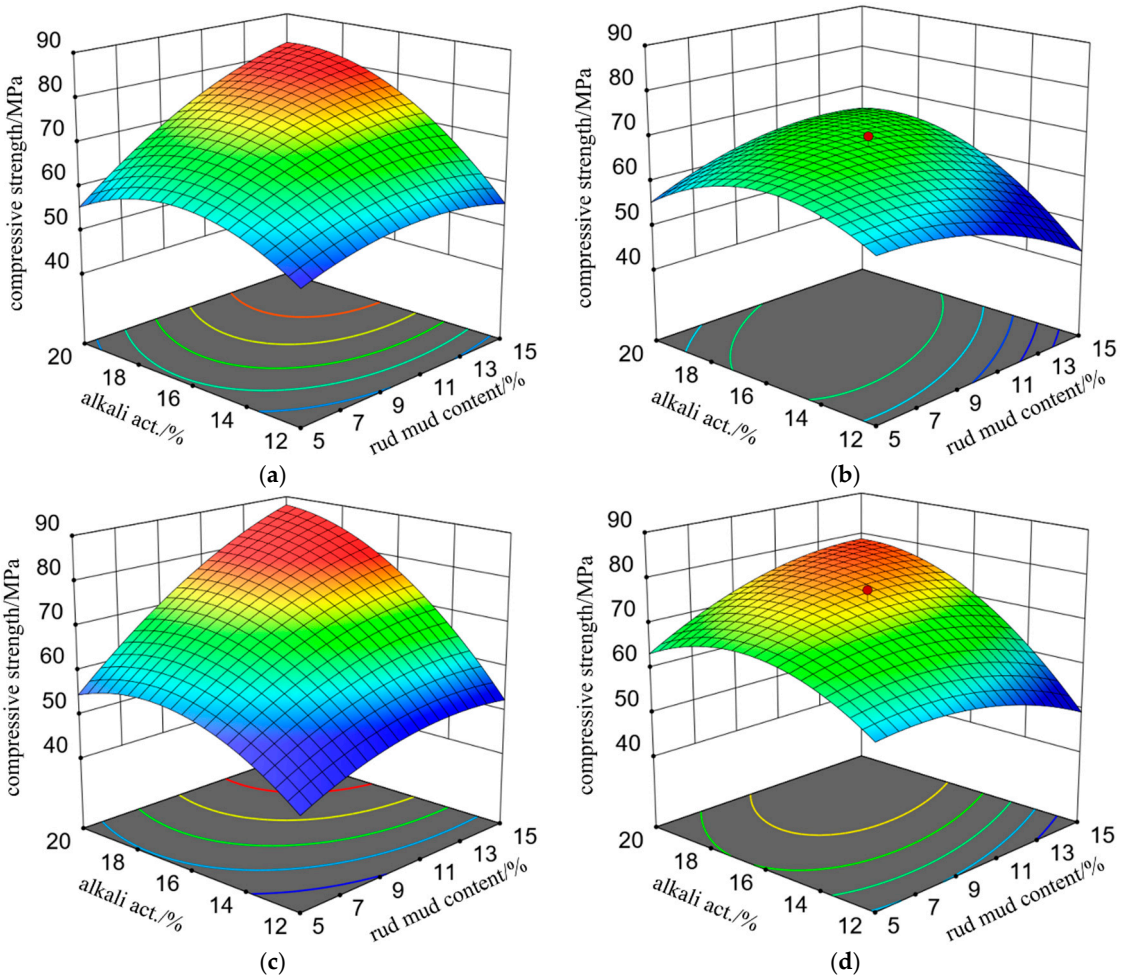


Figure 4. Effects of alkali activator and red mud content on 28-day compressive strength of samples under different conditions. Variable B denotes the volume content of end-hook copper-plated steel fibers (vol.%), and variable D represents the calcination temperature of red mud (°C). (**a**) B = 0; D = 650. (**b**) B = 0; D = 850. (**c**) B = 1.5; D = 650. (**d**) B = 1.5; D = 850.

In summary, the synergistic effects of red mud content and alkali activator dosage significantly influence compressive strength, while individual factor effects dominate the flexural strength behavior. At 0 vol% fiber content and 850 °C calcination temperature, the mechanical properties reach their optimum with an alkali activator dosage of 16% and red mud content of approximately 10%, yielding flexural and compressive strengths of 12.26 MPa and 69.83 MPa, respectively. Compared to the values of 8.7 MPa for flexural strength and 44.2 MPa for compressive strength obtained at 12% alkali activator and 15% red mud content, this represents an increase of 40.92% and 57.99%.

3.4. Microstructural Analysis

3.4.1. XRD Analysis

Figure 5 presents the XRD analysis of alkali-activated red mud–mineral powder composite cementitious materials at curing ages of 3, 7, and 28 days. The phase evolution reveals the effects of different curing ages on hydration reactions and material performances. The main phases include hematite, calcite, C-S-H gel, and C-A-S-H gel. At the 3-day curing age, the diffraction peaks of unreacted minerals (hematite and cancrinite) are prominent, and the calcite peaks also exhibit moderate intensity. The weak diffraction peaks of C-S-H gel and C-A-S-H gel indicate that the initial hydration reactions are dominated by the dissolution of active components, while the formation of hydration products such as

analcime remains in its early stages. At this stage, phase evolution is relatively limited, and the catalytic effect of alkali activation has not been fully manifested. As the curing age extends to 7 days, the diffraction peaks of C-S-H gel and C-A-S-H gel in the XRD patterns significantly intensify, indicating accelerated alkali activation and increased analcime formation. Compared to the 3-day curing age, the diffraction peak intensity of cancrinite shows no significant change, suggesting low participation of this unreacted mineral, which remains predominantly in its original state. Concurrently, the diffraction peak intensity of hematite remains stable, reflecting its low reactivity, yet it does not significantly hinder the formation of hydration products such as analcime. At the 28-day curing age, the diffraction peaks of C-S-H gel and C-A-S-H gel further intensify and stabilize, reflecting the gradual maturation of hydration reactions. The substantial generation of analcime and other hydration products is a critical factor in the late-stage performance improvement. However, the diffraction peaks of cancrinite and hematite remain distinct, indicating their limited chemical reactivity during alkali activation and minimal contribution to phase evolution.

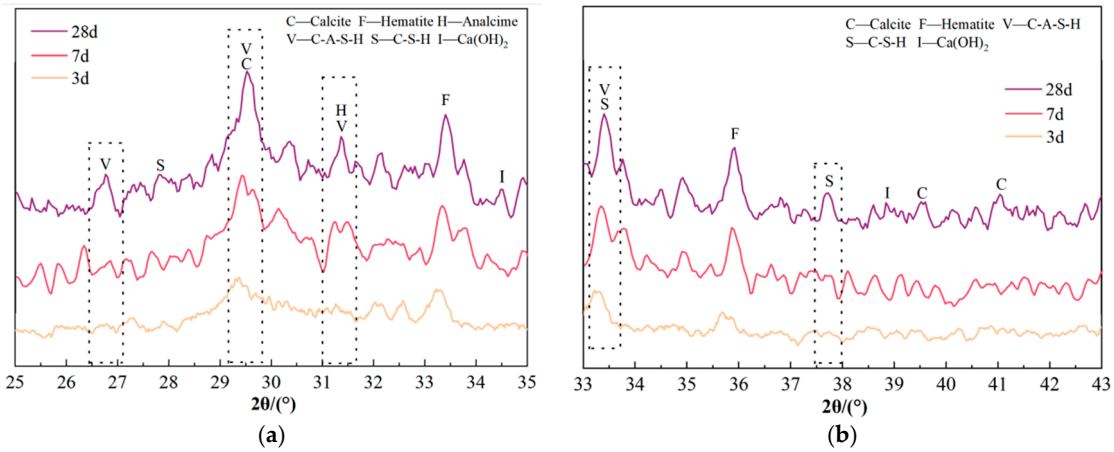


Figure 5. XRD analysis of hydration products of alkali-activated red mud composite cementitious materials at different ages. (**a**) 2θ:25~35°; (**b**) 2θ:33~43°.

In conclusion, with the extension of the curing age, the intensities of the diffraction peaks of C-S-H and C-A-S-H gels increase, indicating an increase in their production amounts which is beneficial for improving the overall compactness of the composite material. The C-S-H gel, as the main hydration product, fills pores and enhances the matrix strength; due to the introduction of Al elements, C-A-S-H forms a stable three-dimensional structure, improving toughness and crack resistance. The continuous generation and expansion of the above-mentioned gel system from 7 days to 28 days are precisely the microscopic basis for the compressive strength of the material to increase from 8.88 MPa to 12.26 MPa.

3.4.2. SEM Analysis

Through the analysis of the SEM results presented in Figure 6 and the EDS data shown in Table 9 in conjunction with the variations in crack width, it is possible to systematically unveil the microstructural evolution of alkali-activated red mud composite cementitious materials at different ages, the formation characteristics of hydration products, as well as their impacts on the compactness and properties of the materials. As pointed out in references [25,26], the C-S-H gel is a composite phase, and the molar ratio of Ca/Si (CaO/SiO_2) thereof ranges from 0.25 to 2.3. The N-A-S-H and C-A-S-H gels consist of aluminate tetrahedra and alkali metal ions. Their main structures are formed via the polycondensation of aluminates with different Al/Si ratios (the Al/Si ratio is between

0.25 and 1). Through the analysis of the SEM results presented in Figure 6 and the EDS data shown in Table 5, in conjunction with the variations in crack width, it is possible to systematically unveil the microstructural evolution of alkali-activated red mud composite cementitious materials at different ages, the formation characteristics of hydration products, as well as their impacts on the compactness and properties of the materials. EDS analysis shows that the molar percentages of O, Si, and Ca in region A are 30.50%, 9.93%, and 8.68%, respectively, and the Ca/Si and Al/Si ratios are 0.87 and 0.49, respectively, reflecting the initial state of the formation of hydration products, which is consistent with the weak intensity of the early hydration product diffraction peaks in the XRD pattern. As the age increases to 7 days, the formation of hydration products significantly increases, and the microstructure undergoes significant changes. The SEM image (b) shows that flocculent and network-like gels gradually cover more areas of the sample surface, filling cracks and pores, and the crack width reduces to 0.48 μm and 0.26 μm, significantly improving the compactness of the material. EDS data further verify this change, with the molar percentages of O, Si, Ca, and Al in region D being 23.10%, 11.21%, 21.63%, and 5.41%, respectively, and the Ca/Si and Al/Si ratios being 1.92 and 0.48, respectively. This indicates that the formation of calcium silicate hydrate gel and geopolymer gel has significantly increased in quantity and uniformity of distribution, and their filling and strengthening effects on the sample structure are more obvious. At the age of 28 days, the hydration reaction tends to be complete. The SEM image (c) shows that the sample surface is almost completely covered by flocculent and network-like gels, the crack width further reduces to 0.13 μm, the porosity is significantly reduced, and the microstructure compactness reaches the best state. EDS analysis shows that the molar percentage of O in region G increases to 48.96%, the proportions of Si and Al are 14.90% and 11.31%, respectively, and the Ca content decreases to 6.53%, with the Ca/Si and Al/Si ratios being 0.44 and 0.76, respectively. The Ca/Si ratio (0.44) observed in this study is highly consistent with the results reported by Zhu et al. [25] in their research on the structural stability of C-S-H. Their study pointed out that a relatively low Ca/Si ratio is conducive to the formation of a dense and homogeneous gel network, thereby improving the compressive performance. In addition, Salami et al. [26] reported that when the Al/Si ratio is controlled between 0.5 and 0.8, the connectivity and plasticity of the gel structure can be significantly enhanced, thereby improving the toughness of the material. The Al/Si ratio of our sample at the 28-day curing age is 0.76, which is consistent with their conclusion. It reflects that the C-A-S-H gel formed in this study not only helps to fill cracks but also promotes the increase in flexural strength by improving the strength of the ITZ, which confirms the toughening effect of the fiber-gel coupling structure.

Table 9. The molar mass percentage of main elements in hydration products of alkali-activated red mud composite cementitious materials at different ages.

Age Period	Region	O	Fe	Si	Ca	AI	Na	C	Mg	S	K
3-day	A	30.50	40.87	9.93	8.68	4.89	2.52	1.68	0.41	0.35	0.17
	B	19.50	1.88	26.58	40.80	5.63	1.97	1.53	0.23	1.06	0.82
	C	6.06	32.61	22.24	32.08	4.22	0.65	0.15	0.15	1.17	0.67
7-day	D	23.10	15.34	11.21	21.63	5.41	1.90	3.60	0.43	1.68	0.70
	E	11.26	41.53	12.94	19.91	6.97	0.36	4.91	0.37	0.73	1.02
	F	9.24	43.69	10.06	17.87	6.35	4.84	5.11	0.38	0.23	2.23
28-day	G	48.96	9.35	14.90	6.53	11.31	5.78	2.01	0.31	0.55	0.3
	H	39.65	0.60	17.08	21.42	4.53	11.06	3.43	1.04	0.65	0.55
	I	47.99	0.68	12.87	18.98	3.03	9.65	6.17	0.16	0.09	0.38

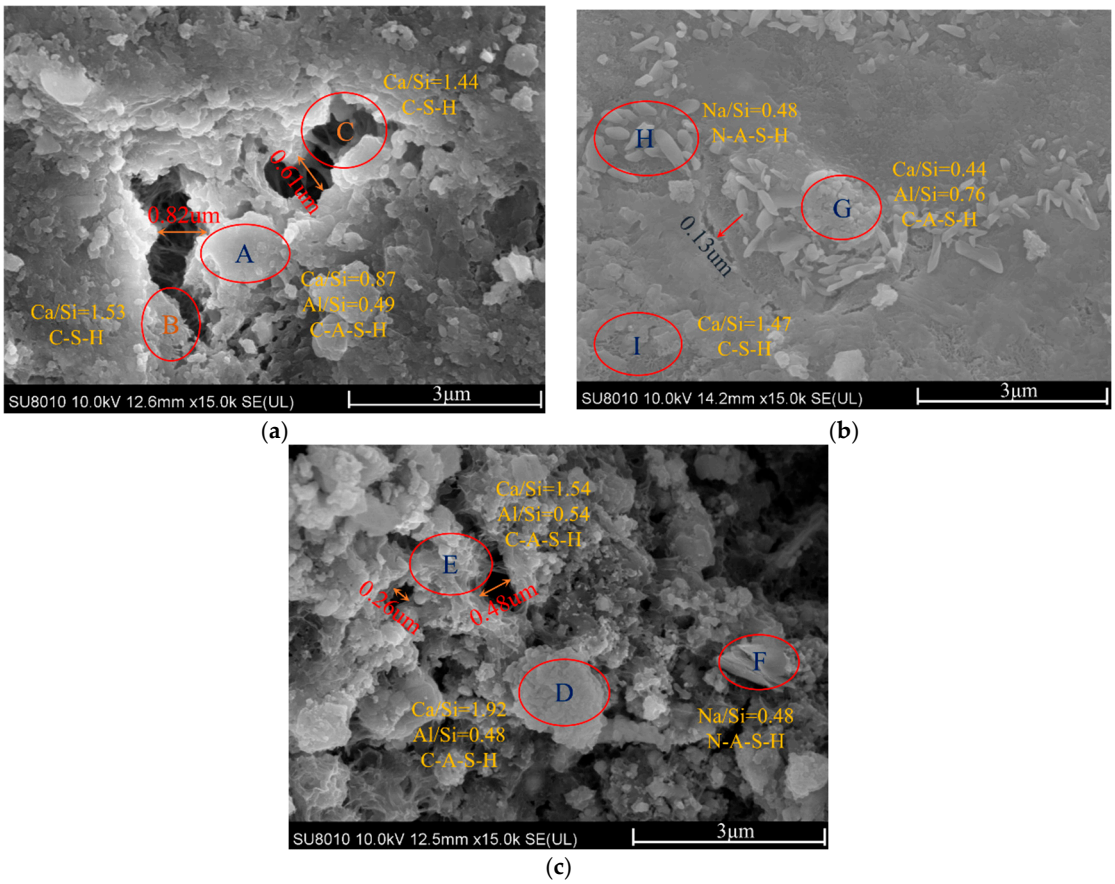


Figure 6. SEM analysis of alkali-activated red mud composite cementitious materials at different ages. (**a**) 3-day; (**b**) 7-day; (**c**) 28-day.

During the period from 3 days to 28 days of age, the crack widths gradually decreased from 0.82 μm and 0.61 μm to 0.13 μm. This indicates that as the hydration reaction progresses, the hydration products gradually fill the cracks and pores, significantly enhancing the compactness of the material and the uniformity of its microstructure. The EDS data suggest that the formation characteristics of hydration products at different ages are closely associated with the changes in the microstructure. The progressive reduction in the crack width is the result of the combined effects of calcium silicate hydrate gel and geopolymer gel. These gels fill the cracks and improve the connectivity, thereby endowing the specimens with higher strength and compactness. Thus, based on the EDS and SEM results, in the samples at the 28 d curing age, the Ca/Si ratio stably remains at approximately 0.44, and the Al/Si ratio reaches 0.76. The gel system exhibits characteristics of high density and uniform distribution. Meanwhile, the crack width is significantly reduced to 0.13 μm, indicating that the material structure tends to be stable. These microstructural features show a clear positive correlation with the macroscopic mechanical properties, explaining why the specimens can achieve a flexural strength of 69.83 MPa and a compressive strength of 12.26 MPa at this age, and providing support for establishing the "composition–structure–property" correlation mechanism.

4. Conclusions

In this study, red mud and mineral powder were used as the main raw materials. The response surface experimental design method was employed to systematically examine the influence of four factors, namely the content of red mud, the volume content of steel fibers, the content of alkali activator, and the calcination temperature of red mud, on the mechanical properties of the composite cementitious materials. Moreover, the microscopic

structural characteristics were explored by means of XRD and SEM. The main findings are as follows:

1. The Box–Behnken response surface design was employed to optimize the red mud–slag powder composite cementitious material. The results showed that the content of red mud and the content of alkali activator were the main factors influencing the compressive strength and flexural strength. The established response surface regression model exhibited high prediction accuracy and excellent fitting performance, and could effectively guide the optimization of actual mix proportions.
2. Under the conditions of a fiber content of 0 vol.% and a calcination temperature of 850 °C, when the content of red mud is 10% and the content of alkali activator is 16%, the flexural strength and compressive strength of the specimens reach 12.26 MPa and 69.83 MPa, respectively. Compared with other combinations, the comprehensive performance has been significantly enhanced, which demonstrates that there is a synergistic strengthening effect between the raw material ratios of red mud and mineral powder and the activation conditions.
3. The hydration reaction of the alkali-activated red mud–slag powder composite material intensifies continuously with the progression of the age. In the early stage, the hydration products consist of a small amount of C-S-H and C-A-S-H gels. As time goes on, they gradually transform into a dense structure mainly composed of analcime and geopolymer gels. These products effectively fill the pores and cracks, significantly improving the compactness and microscopic uniformity of the material. This provides a solid microscopic basis for the enhancement of the material's mechanical properties in the later stage.
4. Through comparative analysis with traditional Portland cement, it is found that for the red mud–mineral powder composite cementitious material, its carbon emission per unit product can be reduced by 44.3% compared with that of traditional Portland cement, and the heat energy consumption can be reduced by more than 36.6%. Preliminary cost estimation shows that the production cost of this material is about 47.6% lower than that of ordinary cement, demonstrating good economic efficiency and potential for engineering promotion. For detailed comparison, see Appendix A.

Author Contributions: Investigation, Q.Z.; data curation, J.H.; writing—original draft, C.Y.; writing—review and editing, W.Z. All authors have read and agreed to the published version of the manuscript.

Funding: This research was funded by the National Natural Science Foundation of China, grant number 51708220 (Project: Study on the mechanism of rock mass collapse and the modification of building materials with arsenic sandstone, PI: Dong Jingliang). The APC was not applicable as the journal does not charge article processing fees.

Data Availability Statement: The data presented in this study are not publicly available because no new datasets were created or analyzed in this research apart from the experimental results reported within the article. Further data sharing is not possible due to privacy or ethical restrictions.

Acknowledgments: This work was supported by National Natural Science Foundation of China (51708220). The authors are grateful for their support.

Conflicts of Interest: The authors declare no conflict of interest.

Nomenclature

REM	Response Surface Methodology
C-S-H Gel	Calcium Silicate Hydrate Gel
C-A-S-H Gel	Calcium Aluminosilicate Hydrate Gel
N-A-S-H Gel	Sodium Aluminosilicate Hydrate Gel
XRD	X-ray Diffraction
SEM	Scanning Electron Microscope
EDS	Energy Dispersive Spectroscopy
ITZ	Interfacial Transition Zone

Appendix A. Quantitative Analysis of Environmental Benefits of Red Mud–Mineral Powder Composite Cementitious Material

Indicator Category	Traditional Cementitious Material (P.O42.5)	Red Mud–Mineral Powder Composite Cementitious Material (this study)	Relative Difference or Savings Ratio	Data Source and Explanation
CO_2 Emissions (kg/t)	995.54	554.2	Decrease by approximately 44.3%	Experimental estimation
Thermal Energy Consumption (MJ/t)	1197	759	Decrease by approximately 36.6%	Clinker calcination at 1450 °C vs. red mud calcination at 850 °C
Material Cost (Yuan/t)	420	220	Decrease by approximately 47.6%	Red mud and mineral powder are industrial by-products with low purchase prices
Raw Material Carbon Footprint	High	Low	Significant advantage	Red mud from zero-carbon sources; mineral powder as blast furnace by-product
Industrial Waste Utilization Rate	None	Red mud (30–40%) and mineral powder (30–50%)	Significant improvement	Improve resource utilization rate

References

1. Li, J.; Zheng, F.Q.; Jing, T. Inhibition Mechanism of Liquid Phase Generation in the Calcification and Reduction Process of High-Speed Railway Red Mud. *Sinter. Pelletizing* **2024**, *49*, 88–95.
2. Sun, Z.; Tao, Z.; Li, H.; Pittman, A.S.; Zhou, F.; Zhang, G.; Wu, J.; Cheng, H.; Feng, E.; Chen, Z.; et al. Recovery of rare earth elements, gallium and germanium from fly ash and red mud via ultra-fast flash Joule heating. *Chem. Eng. Sci.* **2025**, *315*, 121879. [CrossRef]
3. Peng, F.G.; Wang, F.X.; Ding, H.; Jia, Y.J. Effect of calcined red mud on the mechanical properties and microstructure of ultra-high performance concrete. *Constr. Build. Mater.* **2025**, *484*, 141891. [CrossRef]
4. Rashidian, S.; Hosseini, A.S.; Korandeh, E.M. Investigation of red mud effects on microsurfacing asphalt performance: Quality enhancement and industrial waste reduction. *Constr. Build. Mater.* **2025**, *483*, 141798. [CrossRef]
5. Zhang, J.F. Analysis of the Resource Utilization Process of Bayer Process Alumina Red Mud. *Metall. Mater.* **2025**, *45*, 34–36.
6. Li, J.H.; Wang, X.T.; Liu, L.L. Guiding Opinions on the Comprehensive Utilization of Bulk Solid Waste during the 14th Five-Year Plan Period. *Gold Sci. Technol.* **2021**, *29*, 286.

7. Tsakiridis, P.E.; Agatzini-Leonardou, S.; Oustadakis, P. Red mud addition in the raw meal for the production of Portland cement clinker. *J. Hazard. Mater.* **2004**, *116*, 103–110. [CrossRef]
8. Zhu, X.; Li, W.; Zhao, H.; Zhang, C. Selective dealkalization of red mud using calcium oxide with pressure leaching. *JOM* **2018**, *2018 70*, 2800–2806.
9. He, M.D.; Huang, P.; Lu, Q. Practice of Producing Cement Clinker by Using Red Mud as a Substitute for Iron Ore in Raw Materials. *Sichuan Cem.* **2014**, *2014*, 33–34.
10. Garanayak, L. Strength effect of alkali activated red mud slag cement in ambient condition. *Mater. Today Proc.* **2021**, *44*, 1437–1443. [CrossRef]
11. Zhao, Y.R.; Chen, P.; Wei, H.J. Preparation of belite-sulfoaluminate cement using fly ash and red mud from the Bayer process. *J. Guilin Univ. Technol.* **2015**, *35*, 581–584.
12. Ren, C.; Wang, W.; Mao, Y.; Yuan, X.; Song, Z.; Sun, J.; Zhao, X. Comparative life cycle assessment of sulfoaluminate clinker production derived from industrial solid wastes and conventional raw materials. *J. Clean. Prod.* **2017**, *167*, 1314–1324. [CrossRef]
13. Liu, J.H.; Zhou, Z.B.; Wu, A.X. Preparation and hydration mechanism of low-concentration Bayer red mud filling materials. *J. Eng. Sci.* **2020**, *42*, 1457–1464.
14. Liu, J.; Li, Z.L.; Zhang, W.Z. Research Progress on the Preparation of Cold-Bonded Artificial Lightweight Aggregates from Industrial Solid Waste Materials. *Mater. Rev.* **2023**, *37*, 131–148.
15. He, A.P.; Xiong, Y.X. Application of Industrial Solid Waste in Concrete. *Resources, Environ. Eng.* **2013**, *27*, 78–81.
16. Ruan, Z.Y.; Wu, P.J.; Wu, A.X. Optimization of Proportions and Hydration Mechanism of Early-Strong Cementitious Materials Based on Refining Slag for Mining. *Chin. J. Nonferrous Met.* **2023**, *33*, 3064–3076.
17. Ren, G.; Wu, H.; Fang, Q.; Liu, J.Z. Effects of steel fiber content and type on static mechanical properties of UHPCC. *Constr. Build. Mater.* **2018**, *163*, 826–839. [CrossRef]
18. Banthia, N.; Gupta, R. Influence of polypropylene fiber geometry on plastic shrinkage cracking in concrete. *Cem. Concr. Res.* **2006**, *36*, 1263–1267. [CrossRef]
19. *GB/T 17671-2021*; Test Method for Compressive Strength of Cement Mortar. ISO Method: Geneva, Switzerland, 2021.
20. *ISO 679:2009*; Cement–Test Methods–Determination of Strength. International Organization for Standardization: Geneva, Switzerland, 2009.
21. Zhou, M.; Bai, J.T.; Guo, L.Z.; Zhang, Y. Optimization of Grouting Material Proportion of Coal Gangue Geopolymer Based on Response Surface Methodology. *Mater. Rep.* **2023**, *37*, 123–131. (In Chinese)
22. Kockal, U.N.; Ozturan, T. Optimization of properties of fly ash aggregates for high-strength lightweight concrete production. *Mater. Des.* **2011**, *32*, 3586–3593. [CrossRef]
23. Teng, L.M.; Zhang, Q.; Wu, J.; Song, Y.C.; Xu, Y.; Liu, J.; Wang, H.T.; Zhao, Y.; Chen, L.; Li, X.; et al. Optimization of response surface methodology for the synthesis NaP type zeolite from cinder. *J. Funct. Mater.* **2022**, *53*, 8214–8220. (In Chinese)
24. Yuan, X.; Shi, Y.; Chen, Y.; Yuan, X.H.; Guan, H.; Lu, F.; Chen, X. Effect of Steel Fiber Content on Mechanical Properties of Alkali-Slag Concrete. *J. Xinyang Norm. Univ. (Nat. Sci. Ed.)* **2023**, *36*, 656–662.
25. Zhu, X.; Qian, C.; He, B. Experimental study on the stability of CSH nanostructures with varying bulk CaO/SiO2 ratios under cryogenic attack. *Cem. Concr. Res.* **2020**, *135*, 106114. [CrossRef]
26. Salami, B.A.; Maslehuddin, M.; Johari, M.A.M.; Mohamed, H.D.; Ahmad, Z.A. Effect of alkaline activator ratio on the compressive strength response of POFA-EACC mortar subjected to elevated temperature. *Mater. High Temp.* **2021**, *38*, 166–176. [CrossRef]

Disclaimer/Publisher's Note: The statements, opinions and data contained in all publications are solely those of the individual author(s) and contributor(s) and not of MDPI and/or the editor(s). MDPI and/or the editor(s) disclaim responsibility for any injury to people or property resulting from any ideas, methods, instructions or products referred to in the content.